

Improved performance of InAs/GaSb Strained Layer Superlattice detectors with SU-8 passivation

H.S. Kim, E. Plis, S. Myers, A. Khoshakhlagh, N. Gautam, M. N. Kutty,
Y. D. Sharma, L. R. Dawson and S. Krishna*

Center for High Technology Materials, Department of Electrical and Computer Engineering,
University of New Mexico, Albuquerque, NM 87106

ABSTRACT

We report on surface passivation using SU-8 for type-II InAs/GaSb strained layers superlattice (SLS) detectors with a PIN design operating in mid-wave infrared (MWIR) spectral region ($\lambda_{50\% \text{ cut-off}} \sim 4.4 \mu\text{m}$). Material growth and characterization, single pixel device fabrication and testing, as well as focal plane array (FPA) processing are described. High quality strain-balanced SLS material with FWHM of 1st SLS satellite peak of 36 arcsec is demonstrated. The electrical and optical performance of devices passivated with SU-8 are reported and compared with those of unpassivated devices. The dark current density of a single pixel device with SU-8 passivation showed four orders of magnitude reduction compared to the device without any passivation. At 77K, the zero-bias responsivity and detectivity are equal to 1.1 A/W and 4×10^{12} Jones at $4\mu\text{m}$, respectively, for the SU-8 passivated test pixel on the focal plane array.

Keywords: Infrared detectors, InAs/(In,Ga)Sb type-II superlattices, PIN detector, focal plane array, passivation, SU-8

1. INTRODUCTION

Infrared (IR) single element detectors and focal plane arrays (FPAs) are widely used in a variety of fields, including medical diagnostics, climatology, terrestrial pollution monitoring, defense and security. Presently, the most widely used detectors for these applications are bulk InSb (3-5 μm IR wavelength range, MWIR), mercury cadmium telluride (MCT) and intersubband quantum well infrared (QWIP) detectors (8-14 μm IR wavelength range, LWIR) or Si:As Blocked Impurity Band (BIB) detectors (beyond 14 μm , very long wavelength IR, VLWIR). InSb detectors operate at cryogenic temperatures (77K-120K) in order to obtain high signal-to-noise ratio. The low-bandgap MCT alloys are sensitive to small changes in the alloy composition ratio, and poses short lifetimes due to strong Auger recombination rates. Moreover, MCT detectors are characterized by low electron effective mass resulting in excessive dark current due to tunneling [1]. Lack of spatial uniformity over a large area is also an issue for MCT devices. QWIPs have larger dark currents and lower quantum efficiency compared to the interband devices. A significant disadvantage of BIB devices is very low operation temperature (12K) [2], which requires sophisticated multi-stage cooling system.

Type-II short period InAs/(In,Ga)Sb strained layer superlattices (SLSs) have gained a lot of interest over the past few decades as a possible alternative to the present-day infrared (IR) detection systems. Investigation of InAs/(In,Ga)Sb SLSs started in 1970s by Sai-Halasz, Tsu and Esaki [3]. A decade later, Smith and Mailhot [4] proposed this material system for IR detection. The InAs/ (In,Ga)Sb SLSs consist of alternating layers of nanoscale materials whose thicknesses vary from 4-20 nm. These heterostructures have a type-II band alignment such that the conduction band of InAs layer is lower than the valence band of GaSb layer. Electrons and holes localized in InAs and (In,Ga)Sb layers of SLS, respectively. The overlap of electron (hole) wave functions between adjacent InAs ((In,Ga)Sb) layers results in the formation of an electron (hole) minibands in the conduction (valence) band. Optical transition between the highest hole (heavy-hole) and the lowest conduction minibands is employed for the detection of incoming IR radiation. The effective bandgap of the InAs/ (In,Ga)Sb SLSs can be tailored from $3\mu\text{m}$ to $30 \mu\text{m}$ by varying thickness of constituent layers thus allowing fabrication of devices with operating wavelengths spanning the entire IR region. Detectors operating MWIR [5-10], LWIR [11-14], and VLWIR [15, 16] spectral ranges were reported by different research groups.

* skrishna@chtm.unm.edu, phone + 1 505 272 7892, fax + 1 505 272 7801

The thin SLS constituent layers provide a good electron-hole overlap, with the optical matrix elements comparable to those of bulk MCT. (In,Ga)Sb layers of SLS are subjected to biaxial compression causing splitting of light hole and heavy hole minibands in the SLS band structure. Therefore, Auger recombination rates are strongly suppressed relative to bulk MCT [17, 18] leading to improved temperature limits of spectral detectivities compared with MCT detectors [19]. In addition, the larger effective mass in SLS leads to a reduction of tunneling currents compared with MCT detectors of the same bandgap.

Recently, high quality InAs/(In,Ga)Sb SLS grown by molecular beam epitaxy (MBE) has demonstrated remarkable progress [20]. However, the performance of SLS-based FPAs has not yet reached the predicted theoretical limits. One of the reasons is the surface leakage currents generated on the sidewalls of devices due to the abrupt termination of the crystal structure. Decreasing the device size (typical pixel dimensions in FPAs is $24\ \mu\text{m} \times 24\ \mu\text{m}$), results in the surface leakage current being a main component of dark current. To overcome this problem, stable and wavelength independent passivation schemes need to be developed. Several methods have been proposed such as chalcogenide passivation (modification of surface by sulphur or selenium atoms) [21-23], overgrowth with larger bandgap material [24], or encapsulation of device sidewalls with Si_3N_4 , SiO_2 , or polyimide layer [25, 26]. These methods are effective in reducing dark current and improving device performance; however, they either complicate the fabrication process of focal plane arrays (FPAs) or alter the device cut-off wavelength.

SU-8 is a high contrast negative photoresist widely used for micromachining and other microelectronic applications [27, 28]. SU-8 contains bisphenol A novolac epoxy resin and photoacid generator as the curing agent. Viscosity of the resist is determined by the solvent, which is γ -butyrolactone (GBL) [29]. There are twelve commercially available formulations of SU-8 with varied viscosities [30], resulting in different film thickness. Upon UV exposure, a strong acid (HCBF_6) is generated which causes the epoxy resin to form structure with a high cross-linking density. Thus, photopolymerized resist shows outstanding chemical and physical robustness. SU-8 is spin-coated on wide range of substrates giving rise to film thicknesses in the range of (0.2-100) μm .

We think, SU-8 is a good candidate for passivation of InAs/GaSb SLS detectors and FPAs since it provides chemically and thermally stable coatings with varied thickness, and, moreover, it can be easily integrated into detector fabrication process. However, no application of SU-8 for passivation purposes was reported so far.

In the presented paper, we first time report on new passivation material, SU-8, intended to improve performance of InAs/GaSb SLS detector and FPA in the MWIR spectral region.

2. MATERIAL GROWTH AND DEVICE FABRICATION

The devices presented in this work were grown on Te-doped epitaxial (100) GaSb substrates by a solid source molecular beam epitaxy (MBE) VG-80 system equipped with SUMO® cells for indium and gallium, and cracker cells for arsenic and antimony. The group-III growth rates were calibrated by monitoring intensity oscillations of the reflected high energy electron diffraction (RHEED) patterns and confirmed by growth of calibration SLS samples with different thickness of SLS period. Detectors based on the p-i-n design consisted of a 365 nm bottom contact layer formed by 8 monolayers (MLs) InAs: Si ($n = 4 \times 10^{18}\ \text{cm}^{-3}$) / 8MLs GaSb followed by a $\sim 1.6\ \mu\text{m}$ thick non-intentionally doped (n.i.d.) absorber region consisted of SLS with the same composition. Structure was terminated by a 98 nm thick SLS region composed of the p-type ($p = 1 \times 10^{18}\ \text{cm}^{-3}$) InAs/GaSb:Be SLS with the same composition as bottom contact layer. In order to improve transport of minority carriers in detector structure, top (150 nm thick) and bottom (150 nm thick) parts of absorbing region were doped p- and n-type, respectively, with carrier concentration of $1 \times 10^{17}\ \text{cm}^{-3}$. For the same reason, compositionally graded $\sim 50\ \text{nm}$ thick n (p) SLS regions were grown immediately after (before) bottom (top) contact layers. The heterostructure schematic of the MWIR p-i-n detector is presented in Figure 1 (a).

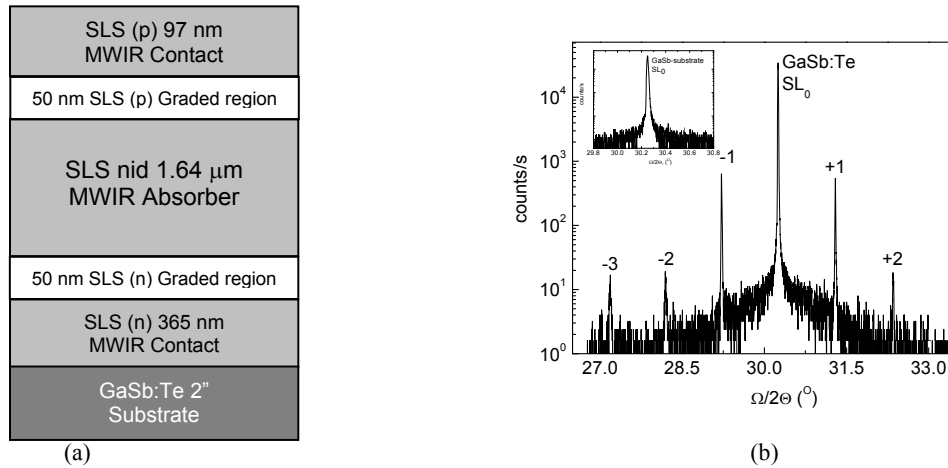


Figure 1. (a) The heterostructure schematic and (b) (004) XRD scan of MWIR SLS p-i-n detector. Inset indicates lattice mismatch between SLS and GaSb substrate is equal to zero

Symmetric (004) X-ray scan was performed on the sample with a Philips double-crystal X-ray diffractometer using the $\text{Cu-K}_{\alpha 1}$ line and is presented in Figure 1 (b). Several orders of satellite SLS peaks are visible. The lattice mismatch between SLS and GaSb substrate is equal to zero, as inset in Figure 1 (b) illustrates. The full width at half maximum (FWHM) of the 1st satellite peak of SLS is equal to 36 arcsec, thus indicating the good crystalline quality of the material. The overall periodicity of the structure, measured by the fringe spacing of the superlattice peaks, is found to be 49.2 Å. This value is in a good agreement with the nominal one (48.6 Å).

Normal incidence single pixel photodiodes were fabricated using standard lithography with apertures ranging from 25-300 μm in diameter. Processing was initiated by mesa etch, which defines the dimension of devices (410 μm x 410 μm). Etching was performed using inductively coupled plasma (ICP) reactor with BCl_3 gas. Resulting etch depth was ~ 2 μm which corresponds to the middle of the bottom contact layer of the detector. Then, an ohmic contacts were evaporated on the bottom and top contact layers using Ti (500 Å) / Pt (500 Å) / Au (3000 Å) in both cases. After contact metallization, some of fabricated devices were wire bonded to a leadless chip carrier for further characterization. The rest of fabricated devices were covered by SU-8 after short (15 seconds) dip in phosphoric acid based solution intended to remove native oxide film formed on the etched mesa sidewalls. Figure 2 shows the mesa sidewalls encapsulated by SU-8 2002 with a thickness of approximately ~1.5 μm.

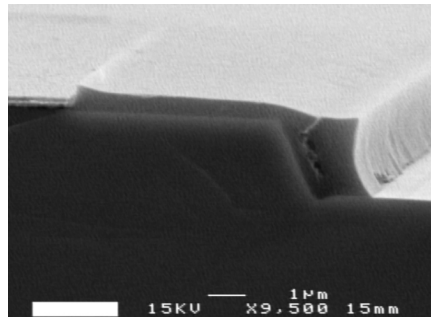


Figure 2. The SEM image of a single pixel PIN SLs diode with SU-8 2002 passivation on the mesa sidewalls

For FPA fabrication a similar processing scheme was utilized. Each processed FPA die consists of 320 x 256 pixels with a 30 μm pitch. An additional test pixel with an area of 24 μm x 24 μm is located at the boundary of the 320x256 FPA which is used for dark current, spectral response, and noise measurements. Processing was initiated by defining 24 μm x 24 μm squares with standard UV photolithography. Then an ICP dry etch to the middle of the bottom contact layer was performed followed by deposition of top and bottom contact metal (Ti (500 \AA) /Pt (500 \AA) /Au (3000 \AA)). Sidewalls of etched mesas were covered with SU-8 2002 for passivation purposes. Finally, to enable well defined indium bumps, an under bump metal (UBM) deposition was conducted using Ti (300 \AA)/Ni (1500 \AA)/Au(500 \AA). Indium metal with a thickness $\sim 2.3 \mu\text{m}$ was thermally evaporated on the UBM metal pads. The reflow process was conducted at a temperature of $\sim 200^\circ\text{C}$ to shape an indium bumps with thickness of $\sim 10 \mu\text{m}$. Figure 3 (a, b) shows indium bumps before and after re-flow process. Finally, the FPAs were hybridized to ISC 9705 read-out integrated circuits (ROICs) made by Indigo. To get enough junction power between the ROICs and FPAs, an under fill material was used. Finally, to minimize thermal stress under low temperature and to diminish free carrier absorption from the GaSb substrate, the majority of the substrate was removed from the back side of the FPAs by mechanical polishing.

3. RESULTS AND DISCUSSION

Spectral measurements of single pixel detectors were performed using a Fourier transform IR spectrometer (FTIR) and a Keithley 428 preamplifier. Figure 4 shows the normalized spectral response (obtained by dividing the photocurrent of the SLS detector with that obtained using a pyroelectric detector) for a 300 μm diameter passivated and unpassivated devices for three different temperatures. Measurements were undertaken at applied voltage of - 0.3 V (reverse bias). The cut-off wavelength was shifted from $\sim 4.6 \mu\text{m}$ at 77 K to $\sim 4.9 \mu\text{m}$ at 150 K. We attribute this shift to the change of bandgap as a function of the temperature.

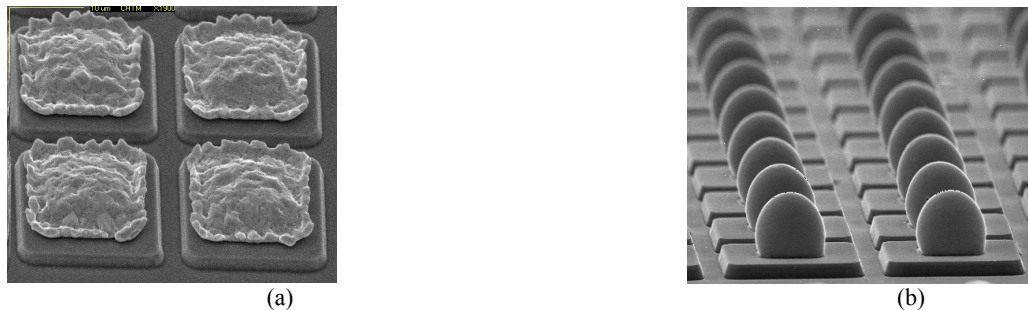


Figure 3. Indium bumps (a) before and (b) after re-flow process

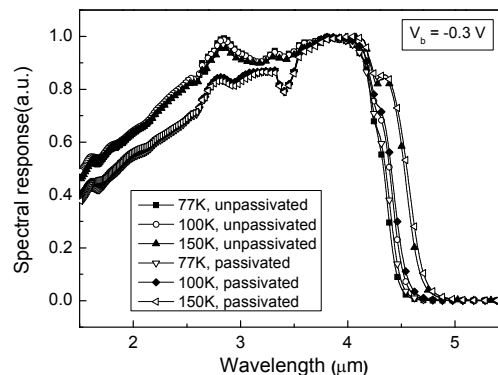


Figure 4. Spectral response of PIN diodes with and without SU-8 passivation at 77, 100, and 150K

Bias dependent dark currents were measured in 77 – 293 K temperature range. The dark current densities for the unpassivated and SU-8 passivated devices measured at 77K are shown in Figure 5. An unpassivated device was characterized three days after processing. Passivated device was measured immediately after passivation and four weeks later. No considerable degradation of the device performance was observed indicating a good long-term stability of SU-8 passivation. Passivated device demonstrated a four orders of magnitude reduction in dark current density compared with unpassivated one (from $\sim 8 \times 10^{-3} \text{ A/cm}^2$ to $\sim 5 \times 10^{-7} \text{ A/cm}^2$) at the same value of applied bias ($V_b = -0.3 \text{ V}$). Dynamic impedance-area product at zero bias R_0A as a function of temperature was calculated based on dark current data for unpassivated and passivated devices. At 77K, R_0A was equal to $1.5 \times 10^3 \Omega \cdot \text{cm}^2$ and $2.3 \times 10^5 \Omega \cdot \text{cm}^2$ for unpassivated and passivated devices, respectively.

To illustrate the relationship between the temperature and dark current, the dark current density at -0.3V is plotted as a function of inverse temperature in Figure 6. The SU-8 passivated device showed an Arrhenius type behavior at high temperatures, indicating that the dominant dark current mechanism is bulk diffusion. The calculated activation energy is 0.255eV which is close to the expected value of the bandgap.

Low-temperature (77K) dark current density of FPA test pixel with area of $24 \mu\text{m} \times 24 \mu\text{m}$ was also measured and shown in Figure 7. At -0.3 V of applied bias, dark current density was equal to $3.4 \times 10^{-6} \text{ A/cm}^2$, which is approximately factor of 7 higher than dark current density measured on passivated single pixel device at the same value of applied bias ($\sim 5 \times 10^{-7} \text{ A/cm}^2$). We attribute this degradation to the additional steps in FPA fabrication, particularly, reflow process, hybridization, underfill process and mechanical thinning of substrate, which induce a lot of stress on the FPA. Thus, surface defect density may be increased degrading the device performance. However, the demonstrated level of FPA dark current is sufficient for FPA imaging and demonstrates that SU-8 is a promising material for FPA passivation. The inset in Figure 7 shows the Arrhenius plot of the temperature dependent dark current density from which the activation energy for device was extracted and it is equal to 245 meV under -0.3 V of applied bias.

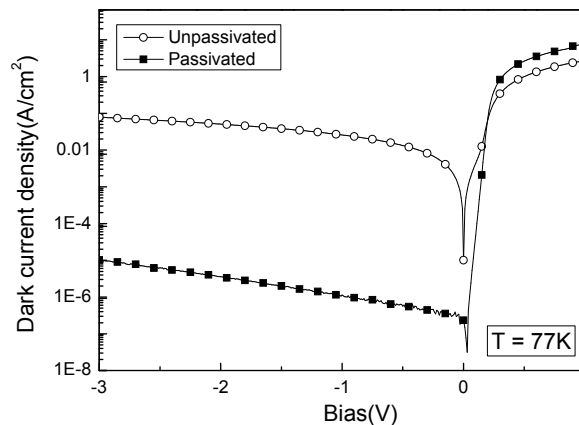


Figure 5. Dark current density for the unpassivated and passivated device measured at 77K. Passivated device demonstrated a four order of magnitude reduction in dark current density under a reverse bias of 0.3 V

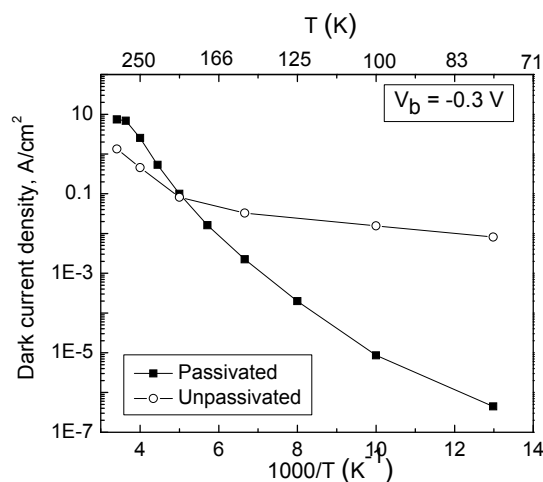


Figure 6. Temperature dependant dark current density of unpassivated and passivated devices measured under reverse bias of 0.3V.

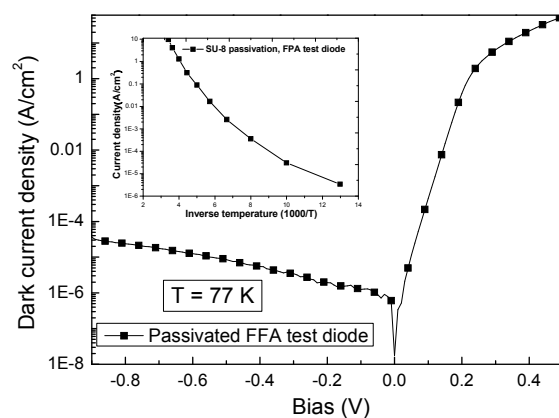


Figure 7. Dark current density for FPA test diode as a function of bias. The inset shows temperature dependence of dark current density measured at -0.3 V

The spectral response of the single FPA pixel with area of $24 \times 24 \mu\text{m}^2$ is shown in Figure 8. The high frequency modulation in the measured spectrum can be noted. It is due to Fabry-Perot interference patterns caused by the residual substrate thickness. These oscillations can be used to calculate the thickness of the residual substrate:

$$d = \frac{m}{2n\Delta\nu} \quad (1)$$

where m is number of fringes in wavenumber region used; d is the residual substrate thickness; n refractive index of GaSb; $\Delta\nu$ is frequency difference. Assuming the refractive index of $n\text{GaSb} = 3.5$, the the thickness d of residual GaSb substrate is equal to $\sim 39 \mu\text{m}$.

For the future, we are planning to include AlGaSb etch stop layer as an intermediate layer between GaSb substrate and detector structure. It will enable complete removal of GaSb substrate using chemical etching and, in turn, eliminate interference patterns from spectral response of SLS FPAs.

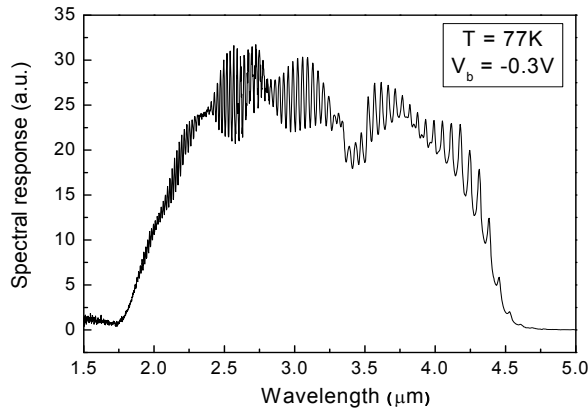


Figure 8. Spectral response of the FPA test pixel under reverse bias of 0.3 V measure at 77K

The responsivity of the FPA test diode was measured using a calibrated blackbody source at 800°C, 800 Hz optical chopper, SR 770 FFT Network signal analyzer and Keithly 428 preamplifier. The background was a 300K scene under $f/2$ illumination. Figure 9 (a) shows the responsivity of the FPA pixel at 77K. The zero-bias responsivity observed was ~ 1.3 A/W and the highest responsivity was equal to ~ 1.1 A/W at the reverse bias of 0.3 V at 4.0 μm .

The specific detectivity D^* was calculated using the following equation:

$$D^* = \frac{R}{\sqrt{2qJ + (4kT)/(R_d A_d)}} \quad (2)$$

where R is the responsivity, q is the electronic charge, J is the dark current density, k is the Boltzmann constant, T is the temperature of the device, $R_d A_d$ is the dynamic impedance-area product where A_d is the electrical area of the diode (24 $\mu\text{m} \times 24 \mu\text{m}$). Low-temperature (77K) D^* calculated at 4 μm as a function of applied bias is shown in Figure 9 (b). The highest value of D^* was equal $\sim 4 \times 10^{12}$ Jones at zero bias.

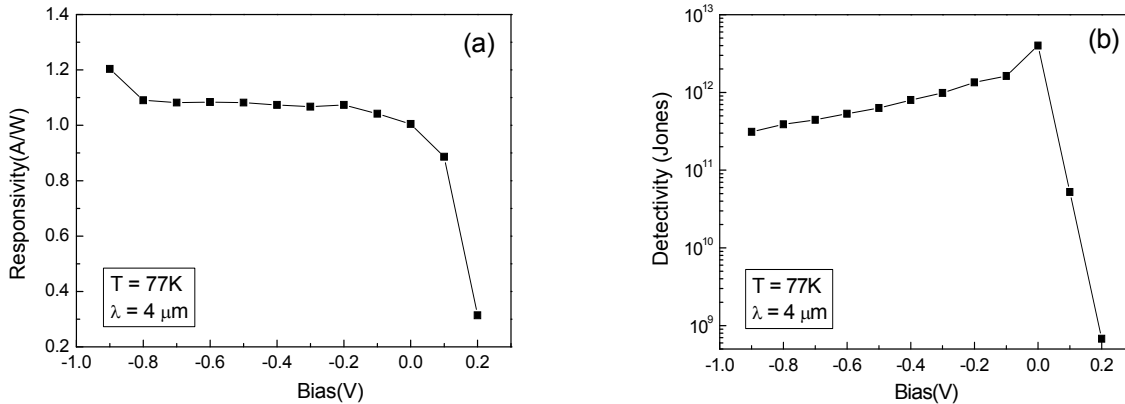


Figure 9. (a) The responsivity of 24 $\mu\text{m} \times 24 \mu\text{m}$ FPA test pixel vs applied bias (b) Specific detectivity D^* as a function of applied bias calculated for the same FPA test pixel. Measurements were undertaken at 77K and 4 μm .

4. SUMMARY AND CONCLUSION

In conclusion, we have demonstrated improved performance of MWIR ($\lambda_{50\% \text{ cut-off}} \sim 4.4 \mu\text{m}$) single pixel detectors with p-i-n design and FPAs based on InAs/GaSb SLS due to SU-8 passivation. Grown SLS has demonstrated the zero lattice mismatch to GaSb substrate and narrow SLS peaks (FWHM of 1st SLS peak was 36 arcsecs), which is an indicator of very good material quality.

Comparison of unpassivated and SU-8 passivated single pixel devices showed a four orders of magnitude reduction in dark current density (from $\sim 8 \times 10^{-3} \text{ A/cm}^2$ to $\sim 5 \times 10^{-7} \text{ A/cm}^2$) at the same value of applied bias ($V_b = -0.3 \text{ V}$). This reduction of dark current attributed to suppression of surface leakage currents. Dynamic impedance-area product at zero bias R_0A as a function of temperature was calculated based on dark current data for unpassivated and passivated devices. At 77K, R_0A was equal to $1.5 \times 10^3 \Omega\text{-cm}^2$ and $2.3 \times 10^5 \Omega\text{-cm}^2$ for unpassivated and passivated devices, respectively.

The FPA test pixel passivated with SU-8 showed reduction of dark current density by three orders of magnitude compared to a non-passivated diode (from $8 \times 10^{-3} \text{ A/cm}^2$ to $3.4 \times 10^{-6} \text{ A/cm}^2$) at -0.3 V of applied bias. The responsivity R and specific detectivity D^* of the FPA test pixel were measured at $4 \mu\text{m}$ and 77K. The zero-bias responsivity was equal to $\sim 1.1 \text{ A/W}$, and corresponding D^* was estimated to $\sim 4 \times 10^{12}$ Jones.

5. ACKNOWLEDGEMENTS

Support from AFOSR Grant FA9550-09-10231, AFRL Grant FA9453-07-C-0171 and KRISS GRL program is acknowledged.

6. REFERENCES

- [1] A Rogalski, "HgCdTe infrared detector material: history, status and outlook", Rep. Prog. Phys. 68, 2267 (2005)
- [2] D.G. Esaev and S.P. Sinitsa, "Photoelectric Characteristics of Infrared Photodetectors with Blocked Hopping Conduction" Semiconductors, 35, 459 (2001)
- [3] G.A. Sai-Halasz, R. Tsu and L. Esaki, "A new semiconductor superlattice", Appl. Phys. Lett., 30, 651 (1977)
- [4] D. L. Smith and C. Mailhot, "Proposal for strained type II superlattice infrared detectors", J. Appl. Phys. 62, 2545 (1987)
- [5] R. Rehm M. Walther, J. Schmitz, J. Fleibner S. Kopta, F. Fuchs, and W. Cabanski and J. Ziegler, "Growth of InAs/GaSb short-period superlattices for high-resolution mid-wavelength infrared focal plane array detectors" J. Cryst. Growth, 278, 156 (2005).
- [6] E. Plis, S.J. Lee, Zh. Zhu, A. Amtout, and S. Krishna, "InAs/GaSb Superlattice Detectors Operating at Room Temperature," IEEE J SEL TOP QUANT, 12, 1269 (2006)
- [7] E. Plis, J. B. Rodriguez, H. S. Kim, G. Bishop, Y. D. Sharma, L. R. Dawson, S. Krishna, S. J. Lee, C. E. Jones and V. Gopal, "Type II InAs/GaSb strain layer superlattice detectors with *p-on-n* polarity" Appl. Phys. Lett., 91, 133512 (2007)
- [8] P. Christol, L. Konczewicz, Y. Cuminal, H. Ait-Kaci, J. B. Rodriguez and A. Joullie, "Electrical properties of short period InAs/GaSb superlattice", Phys. Stat. Sol. C 4, 1494 (2007)
- [9] J. M. Little, S. P. Svensson, W. A. Beck, A. C. Goldberg, S. W. Kennerly, T. Hongsmatip, M. Winn and P. Uppal, "Strained and Unstrained Layer Superlattices for Infrared Detection", J. Appl. Phys. 101, 044514 (2007)
- [10] R. Chaghi, C. Cervera, H. Ait-Kaci, P. Grech, J. B. Rodriguez and P. Christol, "Wet etching and chemical polishing of InAs/GaSb superlattice photodiodes", Semicond. Sci. Technol. 24, 065010 (2009)
- [11] I. Vurgaftman, E.H. Aifer, C.L. Canedy, J.G. Tischler, J.R. Meyer, J.H. Warner, E.M. Jackson, G. Hildebrandt, and G.J. Sullivan, "Graded band gap for dark-current suppression in long-wave infrared W-structured type-II superlattice photodiodes" Appl. Phys. Lett., 89, 121114 (2006)
- [12] B.-M. Nguyen, D. Hoffman, Y. Wei, P.-Y. Delaunay, A. Hood and M. Razeghi, "Very high quantum efficiency in type-II InAs/GaSb superlattice photodiode with cutoff of $12 \mu\text{m}$ " Appl. Phys. Lett. 90, 231108 (2007)
- [13] M. Field, G.J Sullivan, A. Ikhlassi, C. Grein, M.E. Flatté, H. Yang, M. Zhong and M. Weimer, "Electrical and optical performance of InAs/GaSb superlattice LWIR detectors", Proc. of SPIE, 6127, 61270V-1 (2006)

- [14] A. Khoshakhlagh, H. S. Kim, S. Myers, N. Gautam, S. J. Lee, E. Plis, S. K. Noh, L. R. Dawson, and S. Krishna, "Long wavelength InAs/GaSb superlattice detectors based on nBn and pin design," Proc. SPIE, 7298, 72981P (2009)
- [15] M. Razeghi, Y. Wei, A. Gin, G. J. Brown, „Type II InAs/GaSb superlattice photovoltaic detectors with cutoff wavelength approaching $32\ \mu\text{m}$ “, Appl. Phys. Lett., 81, 3675 (2002)
- [16] E.H. Aifer, A. Hood, M. Razeghi, and G.J. Brown, "On the performance and surface passivation of type II InAs/GaSb superlattice photodiodes for the very-long-wavelength infrared", Appl. Phys. Lett., 87, 151113 (2005)
- [17] E. R. Youngblade, J. R. Meyer, C. A. Hoffman, F. J. Bartoli, C. H. Grein, P.M. Young, H. Ehrenreich, R. H. Miles and D. H. Chow, "Auger lifetime enhancement in InAs-Ga_{1-x}In_xSb superlattices", Appl. Phys. Lett. 64, 3160 (1994)
- [18] P. M. Young, C. H. Grein, H. Ehrenreich and R. H. Miles, „Temperature limits on infrared detectivities of InAs/In_xGa_{1-x}Sb superlattices and bulk Hg_xCd_{1-x}Te“, J. Appl. Phys. 74, 4774 (1993)
- [19] C. H. Grein, M. E. Flatte, H. Ehrenreich and R. H. Miles, „Comment on ``Temperature limits on infrared detectivities of InAs/In_xGa_{1-x}Sb superlattices and bulk Hg_xCd_{1-x}Te" [J. Appl. Phys. 74, 4774 (1993)]“, J. Appl. Phys. 77, 4153 (1995)
- [20] A. Rogalski, J. Antoszewski, and L. Faraone, "Third-generation infrared photodetector arrays", J. Appl. Phys. 105, 091101 (2009)
- [21] V.N. Bessolov and M.V. Lebedev, "Chalcogenide passivation of III-V semiconductor surfaces", Semiconductors, 32, 1141 (1998)
- [22] E. Plis, J.B. Rodriguez, S.J. Lee and S. Krishna, "Electrochemical Sulphur passivation of InAs/GaSb SLS detectors", Electron. Lett. 42, 1248 (2006)
- [23] A. Gin, Y. Wei, A. Hood, A. Bajowala, V. Yazdanpanah, M. Razeghi, M. Todrow, "Ammonium sulfide passivation of Type-II InAs/GaSb superlattice photodiodes", Appl. Phys. Lett., 84, 2037 (2006)
- [24] R. Rehm, M. Walther, F. Fuchs, J. Schmitz and J. Fleissner, "Passivation of InAs/(GaIn)Sb short-period superlattice photodiodes with $10\ \mu\text{m}$ cutoff wavelength by epitaxial overgrowth with Al_xGa_{1-x}As_ySb_{1-y}", Appl. Phys. Lett. 86, 173501 (2005)
- [25] A. Gin, Y. Wei, J. Bae, A. Hood, J. Nah and M. Razeghi, "Passivation of type II InAs/GaSb superlattice photodiodes", Thin Solid Films, 447, 489 (2004)
- [26] E. K.-W. Huang, D. Hoffman, B.-M. Nguyen, P.-Y. Delaunay, and M. Razeghi, "Surface leakage reduction in narrow band gap type-II antimonide-based superlattice photodiodes", Appl. Phys. Lett. 94, 053506 (2009)
- [27] E. H. Conradie, D. F. Moore, "SU-8 thick photoresist processing as a functional material for MEMS applications", J. Micromech. Microeng., 12, 368 (2002).
- [28] Thomas A. Anhoj, Anders M. Jorgensen, Dan A. Zauner, and Jörg Hübner, " Optimization of SU-8 processing for integrated optics", Proc. of SPIE, 6110, 611009 (2006)
- [29] M. Shaw, D. Nawrocki, R. Hurditch, and D. Johnson, "Improving the process capability of SU-8", Microsys. Technol. 10, 1 (2003)
- [30] www.microchem.com